Journal of Thermal Science Vol.24, No.1 (2015) 24–29

DOI: 10.1007/s11630-015-0751-9 **Article ID: 1003-2169(2015)01-0024-06**

CFD Simulation of Pulsation Noise in a Small Centrifugal Compressor with Volute and Resonance Tube

Daich Wakaki[1], Yuta Sakuka[1], Yuzo Inokuchi[1], Kosuke Ueda[1], Nobuhiko Yamasaki[1], Akihiro Yamagata[2]

1. Kyushu University, Fukuoka, 819-0395, Japan
2. IHI Corporation, Yokohama, 235-8501, Japan

The rotational frequency tone noise emitted from the automobile turbocharger is called the pulsation noise. The cause of the pulsation noise is not fully understood, but is considered to be due to some manufacturing errors, which is called the mistuning. The effects of the mistuning of the impeller blade on the noise field inside the flow passage of the compressor are numerically investigated. Here, the flow passage includes the volute and duct located downstream of the compressor impeller. Our numerical approach is found to successfully capture the wavelength of the pulsation noise at given rotational speeds by the comparison with the experiments. One of the significant findings is that the noise field of the pulsation noise in the duct is highly one-dimensional although the flow fields are highly three-dimensional.

Keywords: Pulsation Tone Noise, CFD, URANS, Centrifugal Compressor, Turbocharger, Volute

Introduction

The mistuning in the molding processes of the compressor blade sometimes may give rise to the pulsation noise at the rotational frequency (RF) in the automobile turbocharger. The pulsation noise is believed to be amplified by the resonance in the piping system downstream. However there is no research papers published on this specialized topic and this is the motivation of our study. In our previous study [1], we found that the mistuning in the chord length of the impeller blade has a significant impact on the generation of the pulsation noise. The next step of our study is to reveal the characteristics of the sound field in the piping system and this is the objective of this report.

The comprehensive study such as the scaling law on noise [2] is difficult in the field of centrifugal turbomachinery, because the machinery includes pumps, fans, and compressors and their dimensions, rotational speeds, blade shape, existence of the diffuser vanes (stator vanes), and working fluids vary depending on the specific system in which the centrifugal turbomachinery is used, that means that the noise sources and the propagation mechanisms are different from system to system. On the other hand, the scaling law by using the flow coefficient and the pressure coefficient has been successfully used in the manipulation and prediction of the performance data, if the operational range is near the incompressible flow regime.

There are mainly two ways of approaches in predicting the noise from the centrifugal machinery. One method is to solve the noise source directly by using the unsteady CFD [3-5]. However in general computational cost is high and the simulation is limited to the near-field

Received: September 2014
Yuzo Inokuchi: Research Associate

of the impeller. The other method is to solve the resonance in the piping system by using the one-dimensional equations while the turbomachinery itself is treated as a black box of the momentum source [6-8]. In this case, however, the application is limited to relatively low frequencies because the propagation of the plane wave alone is assumed by the use of the one-dimensional equation.

In this report both the whole centrifugal compressor and the resonance tube downstream is solved by using the unsteady CFD to reveal the characteristics of the sound field in the piping system. As far as the authors know, this is the first paper to show such kind of three dimensional sound fields in the piping system of the centrifugal compressor.

Numerical Methods

Geometry of the object

The computational domain is set as shown in Fig.1 to investigate the pulsation noise from the centrifugal compressor of the automobile turbocharger. The compressor impeller has 6 full blades and 6 splitter blades. The outlet diameter of the impeller is 40mm. The air flow accelerated by the impeller is decelerated while passing through the narrow passages of the diffuser and the surrounding volute, and the deceleration causes the pressure rise.

The pulsation noise is the noise that is emitted at the rotational frequency (RF) and has been considered to be caused by the mistuning of the impeller blades in the manufacturing process. In our previous study [1], it is found that the mistuning in the chord length of the blade has the significant influence on the magnitude of the pulsation noise. Therefore also in this study the chord length of the 6 full blades are artificially changed in the circumferential direction in a sinusoidal way with the amplitude of 5% of the chord length, to induce the pulsation noise artificially.

The pulsation noise is believed to be amplified by the resonance in the piping system. Therefore we placed a resonance tube at the exit of the volute and an orifice is set at the end of the resonance tube. The orifice causes artificial reflection of the pressure waves while the air flow passing. The opening ratio of the orifice is set to 0.41, which corresponds to the experiment performed by one of the co-authors at IHI Corporation. The length of the resonance tube is also chosen to match the experimental condition, and is 3 times the diameter of the volute exit.

The noise emitted at the blade passing frequency (BPF) is negligible in our case, because the typical rotational speed of this turbocharger is 170 krpm and its BPF is around 34 kHz, which is beyond the audible range of the human ear.

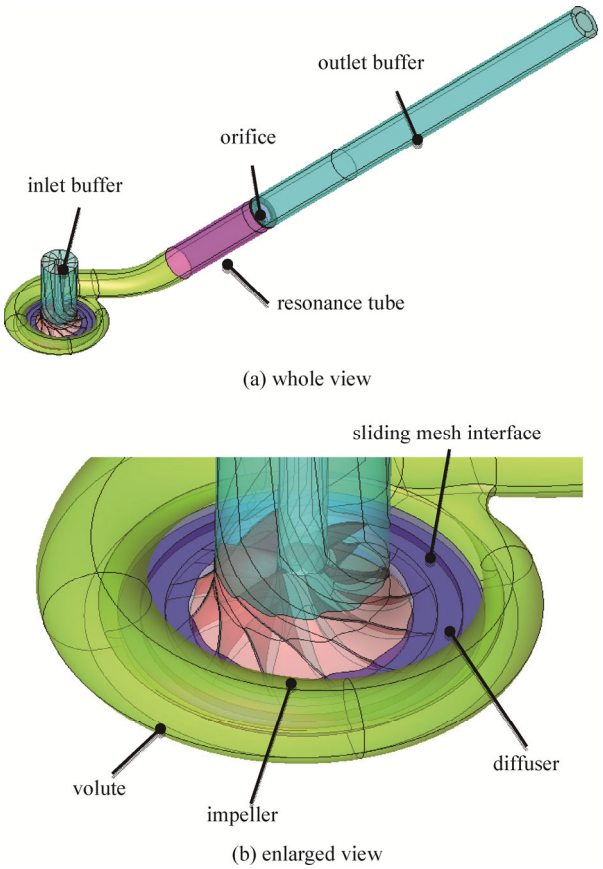

Fig. 1 Computational domain

Operation conditions

The performance curve of our compressor is shown in Fig.2. The abscissa is the normalized volumetric flow rate, and the ordinate is the normalized total pressure ratio between the volute outlet and the impeller inlet. Although the experiments were performed for 6 different rotational speeds between 96 krpm and 222 krpm, only two curves of the measured data at 120 krpm and 200 krpm are shown in the figure. The normalizations of both

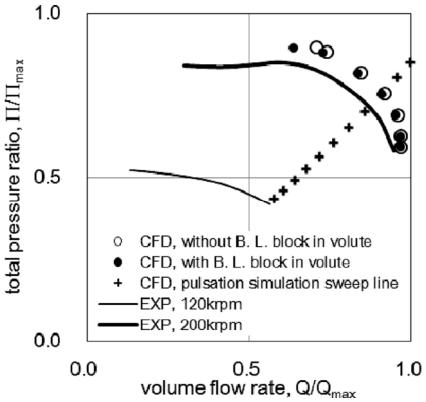

Fig. 2 Simulated conditions on the experimental performance curves

axes of the graph are made by using the maximum values of the measured data at 222 krpm.

Simulated path in our CFD computation is indicated by the cross (+) symbols in Fig.2, which range from 120 krpm to 220 krpm, with 10 krpm increments. Other symbols in this figure will be discussed later.

Fluid flow simulation

A description on the solution methods follows for clarity, although the numerical methods used in this study, including the computational grid topologies and the method to give the mistuning, are described in detail in our previous report [1].

The CFD solver is UPACS-turbo developed by JAXA. The solver uses the cell-centered finite volume method that is formulated for the multi-block structured grid. The governing equation is the system of compressible unsteady Reynolds averaged Navier-Stokes (URANS) equations and the Spalart-Allmaras one-equation turbulence model is used. The convective term is discretized by the Roe scheme and MUSCL extrapolation to the cell interface is made by the 2nd order method, while the viscous term is discretized by the 2nd order centered method.

The time integration is performed by the 1st order Euler implicit method and resulting algebraic system of equations is solved by the matrix-free Gauss-Seidel method. The time step is selected so as the one rotation of the impeller is divided by 3,600.

The buffer areas are added to the upstream of the inlet and the downstream of the outlet, as shown in Fig.1, to reduce unphysical reflections from the boundaries by using the numerical diffusion due to coarse grid spacing. The length of the buffer tube is 1.5 times the inlet casing diameter for the inlet and 11 times the volute exit diameter for the outlet.

Total number of grid points is about 15.7 million, in which 5.0 million points are used for the 12 blade passages including the tip clearances, 1.8 million for the diffuser, 5.4 million for the volute, 1.6 million for the resonance tube , 1.5 million for the inlet buffer, and 0.4 million for the outlet buffer.

The representative length used in this study is the span length of the full blade at the leading edge, which is about 10mm. The casing diameter at the inlet is 3 in this non-dimensional scale. The Reynolds number based on the blade span is 2×10^5 at the 170 krpm case. The typical non-dimensional grid spacing on the blade wall is in the wall normal direction and near the blade leading and trailing edges as well as near the casing and hub walls. The typical y^+ values on the blade wall range from 0.4 to 8 at the 170 krpm case, where large values are found on the casing side. On the diffuser and the volute walls, the typical non-dimensional spacing is 3×10^{-3} and 5×10^{-5} , respectively, and corresponding y^+ values are 7 and 0.1, respectively.

The sliding interface is indicated in Fig.1(b), where rotating frame of reference is connected to the stationary one, while preserving the fluxes between the interface.

The notable changes from our previous report[1] are the addition of the boundary layer block in the volute and addition of the resonance tube. The boundary layer block is added to the volute wall, as shown in Fig.3, with the expectation of improving the prediction accuracy. The number of grid points of the boundary layer block is 1.0 million. The addition of the resonance tube is the main objective of this report and its role is already described in the preceding subsection.

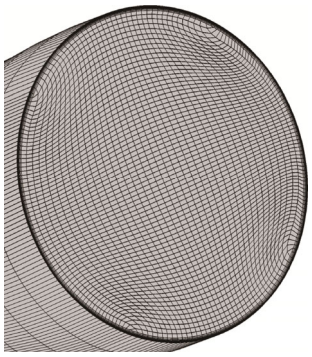

Fig. 3 Cross section of the volute with boundary layer block

Acoustic analysis

The points per wave (PPW) to resolve a wave is 28.6 for the second order scheme [9] and the numerical scheme used in this study is basically second order accurate. The highest RF is about 3.7 kHz (i.e., 220 krpm). The grid spacing in the streamwise direction in the resonance tube is about 0.1, which resolves the fundamental wave at the RF with 80 grid points. It means that up to approximately third harmonics can be accurately resolved with this grid resolution. Higher harmonics such as the BPF can be resolved in a Nyquist sense but the results for such harmonics are inaccurate.

Unsteady pressure fluctuations at the 170 krpm case are sampled at two points shown in Fig. 4. One point is located in the diffuser and the other point is at the exit of

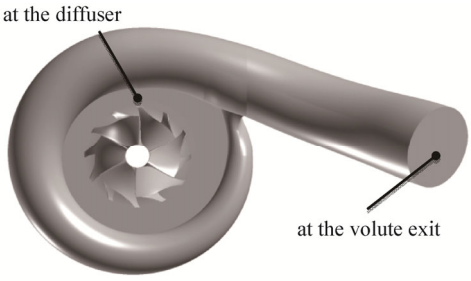

Fig. 4 Data acquisition points of the unsteady pressure fluctuations

the volute. Data are stored during 40 rotations of the impeller with 3600 steps per rotation, which results in the Fourier transformations of the non-dimensional Nyquist frequency of 1800 and non-dimensional frequency resolution of 0.025, where the unit non-dimensional frequency means the rotational frequency.

The wavelengths of the pulsation noise are also compared with the experiments. The virtual pressure taps are placed on the resonance tube along the streamwise direction as in the experiments. The pressure amplitude at the RF is acquired by using the Fourier transformation of the time series data at each virtual pressure tap. The wavelength of the standing wave is estimated by plotting the variation of the pressure amplitude along the pressure taps.

The Fourier transformations are also utilized for the time series data of the pressure fluctuations on the wall, in order to visualize the three-dimensional structure of the standing waves from the diffuser to the resonance tube, by extracting the unsteady pressure amplitude at the RF. In this case due to the disk limitation data are stored during the 10 rotations of the impeller with 3600 steps per rotation.

Results and Discussion

Flow field

A typical flow field is visualized in Fig.5, with streamlines colored by the static pressure. The impeller surface is also colored by the static pressure. The pressure continues to rise from the leading edge of the impeller blade to the trailing edge, from the trailing edge to the diffuser outlet, and from the diffuser outlet to the volute. The pressure rises further in the upstream of the orifice and the flow experiences the sudden pressure drop after passing the orifice. Another feature of this flowfield is the swirling flow that is observed in the volute, which makes the lower pressure area at the center of the swirl. Thus the flowfield has the pressure gradient in the radial direction as well as in the streamwise direction.

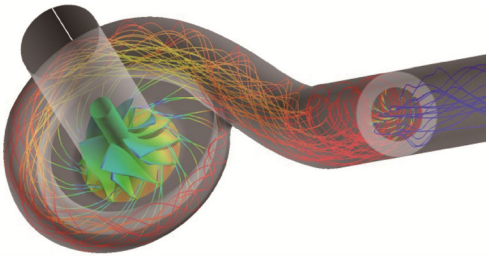

Fig. 5 Typical flowfield represented by streamline colored with static pressure

Comparison with the experimental data

The performance curve obtained from the simulation at 200 krpm is shown in Fig.2 with circle symbols. The black and white circles denote the simulations with and without the boundary layer block in the volute, respectively. The thick line indicates the experimental data at 200 krpm. The simulation captures the performance curve qualitatively, however, the pressure ratio of the compressor is overestimated. The reason of this overestimation is still under investigation. The consideration of the viscous losses at the volute slightly improves the prediction, but no significant effect is observed.

Acoustic field

Figure 6 (a) and (b) shows the time histories of the pressure at the diffuser and at the volute exit, respectively, for the 170 krpm case. The data sampling position is indicated in Fig. 4. The thick and thin lines denote the mistuned and normal cases, respectively. The abscissa is the non-dimensional time normalized by the time for one rotation of the impeller. The ordinate is the non-dimensional static pressure normalized by $\rho_0 c_0^2$, where ρ_0 and c_0

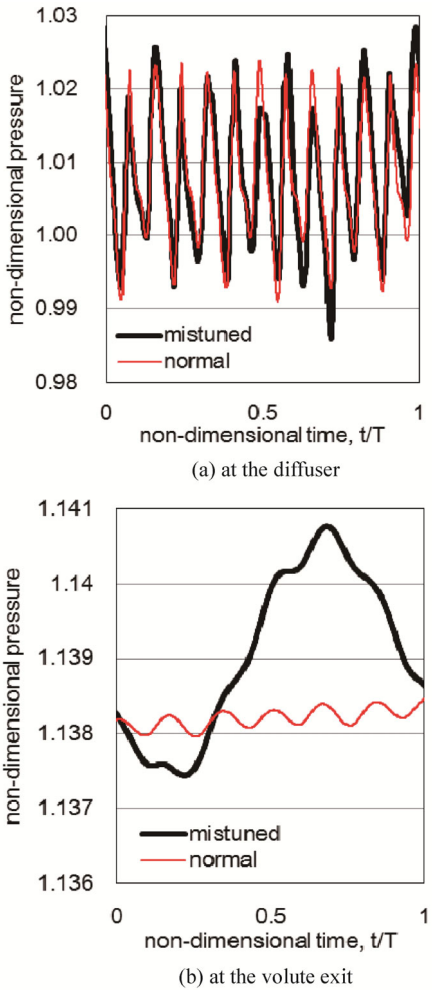

Fig. 6 Non-dimensional pressure fluctuation in unsteady CFD calculation at 170 krpm

denote the stagnation density and the speed of sound at the inlet. The effects of mistuning are not clearly recognized at the diffuser, while at the volute exit the effects can be clearly seen with the elevated mean pressure.

The time series data in Fig. 6 are transformed into the frequency space by the Fourier transformation, in order to investigate the effects of the mistuning on the pulsation noise more clearly. The results are shown in Fig. 7 with the same legend with the previous figure. At the diffuser, the pressure amplitude at the BPF of 12 blades and at the BPF of 6 full blades are large in both the mistuned and normal cases, while the pressure amplitude at the RF is only large in the mistuning case. At the volute exit, the pressure amplitude at the full blade BPF is significantly attenuated from that at the diffuser, while the pressure amplitude in the mistuned case at the RF is not attenuated. The attenuation at the BPF may be caused by the numerical diffusion because in this grid spacing only up to 3 harmonics of the RF can be accurately resolved, as noted earlier in the acoustic analysis subsection.

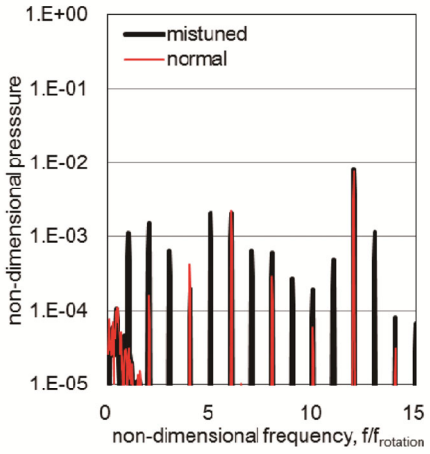

(a) at the diffuser

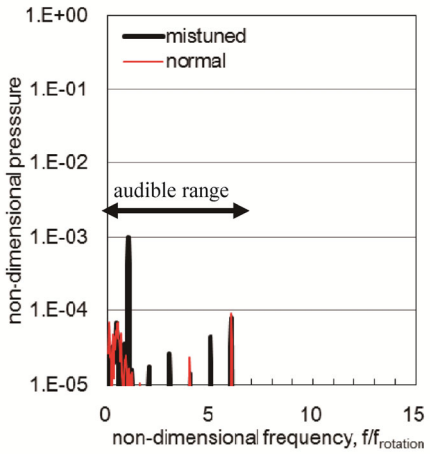

(b) at the volute exit

Fig. 7 Noise spectrum corresponding to Fig. 6

The predicted wavelengths of the pulsation noise are compared with the experimental results in Fig. 8. The simulation runs from the rotational speeds of 120 krpm to 220 krpm, and its sweep path on the performance curve is shown in Fig. 2. It is confirmed that quite good agreement is achieved for the predicted wavelength. The non-dimensional length of the resonance tube is about 10.6, which indicates that the wavelength at the 170 krpm is approximately the same length with the resonance tube.

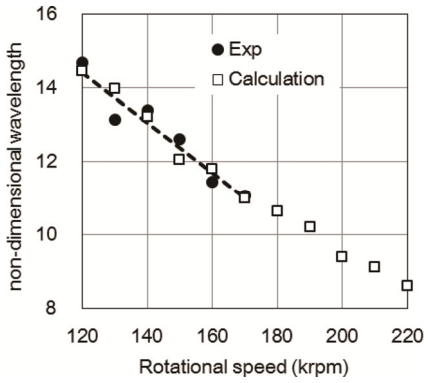

Fig. 8 Non-dimensional wavelength of standing wave in the resonance tube

Finally, three-dimensional structure of the standing waves at the RF is shown in Fig. 9 for the 170 krpm case. It is interesting to note that the standing wave exists not only in the resonance tube, but also in the diffuser and in the volute region. Also, despite the complex flow pattern and the pressure gradient as we already explained by using Fig. 5, It is found that only the plane wave exist from the volute to the resonance tube. The cut-on frequency of the lowest non-plane mode is estimated to be about 5 kHz, by assuming a straight pipe having the diameter of the volute, which corresponds to the RF of 300 krpm. Therefore, as far as the RF is concerned, only the plane wave propagates in the pipe because the operation range of our turbocharger is below 220 krpm.

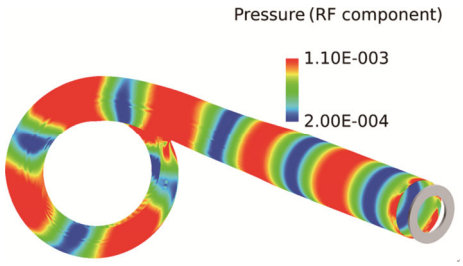

Fig. 9 RF component of unsteady pressure at 170krpm

Conclusions

We performed the unsteady RANS simulations of the centrifugal compressor of the automobile turbocharger to

study the pulsation noise that is caused by the mistuning of the impeller blades and emitted at the rotational frequency. The artificial mistuning is given by the sinusoidal change in the blade chord length in the circumferential direction. The resonance tube is included in the computational domain to simulate the resonance occurred in the actual piping system. The performance curve obtained by the simulation at the rotational speed of 200 krpm agrees with the experimental curve qualitatively. The wavelengths of the standing wave in the resonance tube quantitatively agree with the experimental data. It is found that the resonance occurs not only in the piping system downstream of the volute, but also in the diffuser and the volute. It is also found that in our cases only the plane wave propagates in the piping system, as far as the pulsation noise is concerned, because of the cut-off nature of the sound propagation in ducts.

References

[1] D. Wakaki, Y. Sakuka, N. Yamasaki, and A. Yamagata, Study on Rotational Frequency Noise in a Centrifugal Compressor for Automobile Turbochargers, Journal of Thermal Science 23(1), pp.53–59, (2014).

[2] W. Neise, Application of similarity laws to the blade passage sound of centrifugal fans, Journal of Sound and Vibration, 43(1), pp.61–75, (1975).

[3] F. Shi and H. Tsukamoto, Numerical Study of Pressure Fluctuations Caused by Impeller-Diffuser Interaction in a Diffuser Pump Stage, Journal of Fluids Engineering 123, pp.466–474, (2001).

[4] H. Sun, H. Shin, and S. Lee, Analysis and Optimization of Aerodynamic Noise in a Centrifugal Compressor, Journal of Sound and Vibration 289, pp.999–1018, (2006).

[5] T. Raitor and W. Neise, Sound Generation in Centrifugal Compressors, Journal of Sound and Vibration 314, pp.738–756, (2008).

[6] L. Cremer, The Second Annual Fairey Lecture: The Treatment of Fans as Black Boxes, Journal of Sound and Vibration 16, pp.1–15, (1971).

[7] H. Rämmal and J. Galindo, The Passive Acoustic Effect of Turbo-Compressors, Proceedings of the 9th International Conference on Turbochargers and Turbocharging, London, (2010).

[8] I. Hayashi and S. Kaneko, Pressure Pulsations in Piping System Excited by a Centrifugal Turbomachinery Taking the Damping Characteristics into Consideration, Journal of Fluids and Structures 45, pp.216–234, (2014).

[9] C. Wagner, T. Hüttl, and P. Sagaut, Large-Eddy Simulation for Acoustics, Chapter 5 Numerical Methods, Cambridge University Press, Cambridge, England (2007).